A LONG-TERM COMPARISON OF GPS CARRIER-PHASE FREQUENCY TRANSFER AND TWO-WAY SATELLITE TIME/FREQUENCY TRANSFER

Christine Hackman[†]
JILA, University of Colorado
Boulder, Colorado, USA

Judah Levine
Time and Frequency Division and JILA
National Institute of Standards and Technology and University of Colorado
Boulder, Colorado, USA

Thomas E. Parker
Time and Frequency Division, National Institute of Standards and Technology
Boulder, Colorado, USA

Abstract

GPS carrier-phase frequency transfer (GPSCPFT) and two-way satellite time and frequency transfer (TWSTFT) were performed along three transatlantic links over the 6-month period 29 January – 31 July 2006. The GPSCPFT and TWSTFT results were subtracted in order to estimate the combined uncertainty of the methods. The frequency values obtained from GPSCPFT and TWSTFT agreed at 1.8 to 3.8·10⁻¹⁶ RMS for averaging times of 30 d, with no single value of $y_{GPSCPFT} - y_{TWSTFT}$ exceeding 5.5·10⁻¹⁶. These RMS frequency-accuracy values were equal to or less than the frequency-stability values $\sigma_{y(GPSCPFT) - y(TWSTFT)}(\tau)$ (or TheoBR (τ)) computed for the corresponding averaging times; in general, no frequency bias between GPSCPFT and TWSTFT was observed. The transfer noise of the links varied with time of year, which was especially noticeable in the $y_{GPSCPFT} - y_{TWSTFT}$ values obtained for 10-15 d averaging times: $y_{GPSCPFT} - y_{TWSTFT}$ (10 d) sometimes became as large as 2·10⁻¹⁵. It is not yet clear what caused these variations. RMS ($y_{GPSCPFT} - y_{TWSTFT}$, 10 d) ranged from 0.7 to 1.1·10⁻¹⁵, with these RMS values approximately equal to $\sigma_{y(GPSCPFT) - y(TWSTFT)}(\tau = 10\ d,\ 21\ h)$. Day-boundary discontinuities were not removed or otherwise circumvented in this experiment; we hope to reduce the uncertainty at shorter averaging times (e.g., 10 d) through better management of these discontinuities, along with improved understanding of the seasonal components.

INTRODUCTION

Primary frequency standards (PFSs) can now achieve fractional frequency uncertainties of several parts in 10^{16} in the laboratory [1]. However, to compare the frequency of one PFS to another, or to use a PFS to

---

[†]Address: JILA, University of Colorado, 440 UCB, Boulder, CO 80309-0440 USA; *chackman@jilau1.colorado.edu*

Report Documentation Page

1. REPORT DATE **01 JAN 2007**	2. REPORT TYPE **N/A**	3. DATES COVERED **-**

4. TITLE AND SUBTITLE **A Long-Term Comparison Of Gps Carrierphase Frequency Transfer And Two-Way Satellite Time/Frequency Transfer**	5a. CONTRACT NUMBER
	5b. GRANT NUMBER
	5c. PROGRAM ELEMENT NUMBER
6. AUTHOR(S)	5d. PROJECT NUMBER
	5e. TASK NUMBER
	5f. WORK UNIT NUMBER
7. PERFORMING ORGANIZATION NAME(S) AND ADDRESS(ES) **JILA, University of Colorado Boulder, Colorado, USA**	8. PERFORMING ORGANIZATION REPORT NUMBER
9. SPONSORING/MONITORING AGENCY NAME(S) AND ADDRESS(ES)	10. SPONSOR/MONITOR'S ACRONYM(S)
	11. SPONSOR/MONITOR'S REPORT NUMBER(S)

12. DISTRIBUTION/AVAILABILITY STATEMENT
Approved for public release, distribution unlimited

13. SUPPLEMENTARY NOTES
See also ADM002029., The original document contains color images.

14. ABSTRACT

15. SUBJECT TERMS

16. SECURITY CLASSIFICATION OF:			17. LIMITATION OF ABSTRACT	18. NUMBER OF PAGES	19a. NAME OF RESPONSIBLE PERSON
a. REPORT **unclassified**	b. ABSTRACT **unclassified**	c. THIS PAGE **unclassified**	**UU**	**14**	

calibrate the rate of International Atomic Time (TAI), one must compare the frequency of the local oscillator (LO) used to evaluate the PFS to either the frequency of TAI or to the frequency of the second PFS's LO. A PFS evaluation typically takes 15-30 d; since the uncertainty of the transfer is dominated by phase-noise processes for short averaging times, the uncertainty of a frequency transfer typically decreases with time. In order to take advantage of these small in-lab uncertainties, one must wait for the uncertainty of the frequency transfer to decrease to a few parts in 10^{16}, or even into the 10^{-17} range, if possible.

GPS carrier-phase frequency transfer (GPSCPFT) and two-way satellite time and frequency transfer (TWSTFT) may reach frequency uncertainties in the 10^{-16} s in several days to a few weeks [2-5]. We lack information about the frequency stability of the individual methods at these averaging times. However, the difference of the frequency values yielded by the two techniques represents an estimate of the combined uncertainty of the techniques, assuming that the errors in the two techniques are uncorrelated. We can use the difference of the frequency values obtained to set an upper bound on the uncertainty of either method. Or, for example, we can attribute the combined uncertainty equally to both methods, and thus divide the difference of frequency values by $\sqrt{2}$ and use that result to estimate the frequency uncertainty of either method.

We performed frequency transfer across three transatlantic links using both GPSCPFT and TWSTFT over the 6-month period 29 January – 31 July 2006 (MJDs 53764-947). The primary goal was to examine the long-term combined frequency accuracy and frequency stability of the two methods. The experiment also gave us ample opportunity to examine the agreement between $y_{GPSCPFT}$ and y_{TWSTFT} at averaging times of 10-30 d. This allowed us to assess the suitability of the two systems in evaluating PFSs.

DATA COLLECTION AND ANALYSIS

GPSCPFT and TWSTFT were performed between the National Institute of Standards and Technology (NIST; Boulder, Colorado, USA) and three European laboratories: National Physical Laboratory (NPL; Teddington, U.K.); the Swiss Federal Office of Metrology (METAS; Wabern, Switzerland), and Physikalisch-Technische Bundesanstalt (PTB; Braunschweig, Germany). At each of these laboratories, a single hydrogen maser is used as the frequency reference for both the GPSCPFT and TWSTFT systems. The lengths of the METAS-NIST, NPL-NIST, and PTB-NIST links are 7734, 7118, and 7532 km, respectively.

Figure 1 shows the station locations. The unlabeled blue dots indicate additional GPS receivers (operated by the International GNSS Service (IGS) [6]) whose measurements were included in the GPS data analysis in order to help resolve integer-cycle ambiguities [7]. Table 1 lists the GPS and TWSTFT equipment used at NIST, METAS, NPL, and PTB. Table 2 lists the auxiliary GPS stations used in the analysis. The GPS receivers at NIST and PTB are not the same as those receivers (IGS designations NISU and PTBB) whose tracking data are submitted to the IGS network.

TWSTFT data were collected every 2 h. Each 2 h data collection consisted of 120 1-s measurements; these 120 measurements were reduced to a single time-transfer value according to ITU-R TF.1153-2 [8]. GPS measurements were taken every 30 s and then analyzed – along with tracking data from the auxiliary stations – in 24 h batches using *GIPSY Orbit Analysis and Simulation Software[1]* provided by the Jet Propulsion Laboratory (JPL) [9]. Both carrier-phase and pseudorange measurements were included in the analysis. The data were processed using precise satellite ephemerides and weekly SINEX station coordinates provided by the IGS [10]. SINEX coordinates were typically available for all sites except for IST, PTB, and METAS; the coordinates of these three stations were estimated as part of the analysis. Earth-orientation parameters were obtained from the International Earth Rotation Service (IERS) [11]; ocean-loading coefficients were obtained

---

[1]Specific trade names are used for identification purposes only; no endorsements are implied.

from the Onsala Space Observatory **[12]**.

Figure 1. GPS and TWSTFT sites. The labeled red dots mark the GPSCPFT/TWSTFT sites
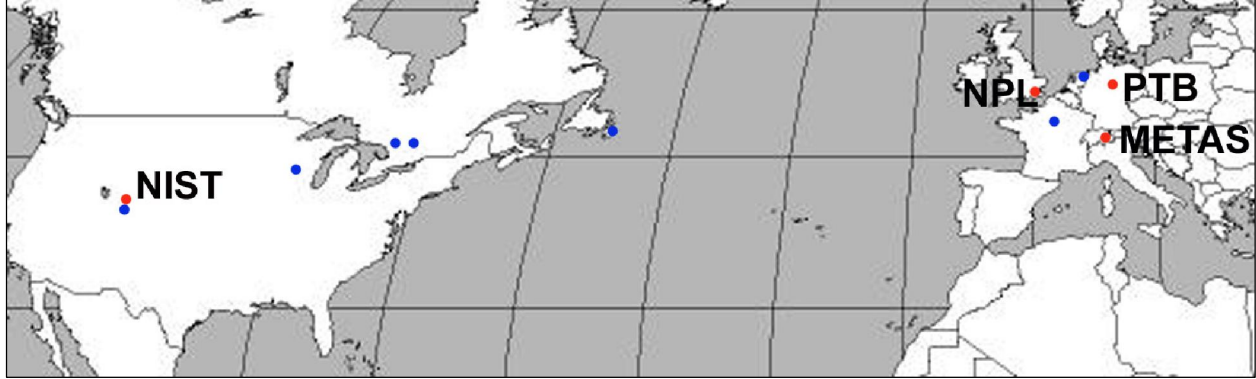
whose frequency-transfer links we examined. NIST = National Institute of Standards and Technology (Boulder, Colorado, USA), METAS = the Swiss Federal Office of Metrology (Wabern, Switzerland), NPL = National Physical Laboratory (Teddington, U.K.), and PTB = Physikalisch-Technische Bundesanstalt (Braunschweig, Germany). The equipment used at these sites is listed in Table 1. The unlabeled blue dots indicate IGS GPS tracking sites whose data were added to the GPS analysis in order to assist in ambiguity resolution **[7]**. Table 2 lists the locations and tracking equipment for these sites.

Table 1. GPS and TWSTFT Hardware Used in Links Studied.

Site	IGS code	GPS		TWSTFT	
		receiver	antenna	modem number[A]	antenna
NIST[B]		AOA SNR-8000 ACT	AOAD/M_T	78	3.7m Andrew
METAS	WAB2	Ashtech Z-XII3T	ASH700936F_C with snow radome	281	1.8m Protline
NPL	NPLD	Ashtech Z-XII3T	AOAD/M_T	74	2.4m ERA
PTB[B]		AOA SNR-8000	AOAD/M_T	03	1.8m Vertex
[A]*All stations used TimeTech SATRE modems.*			[B]*Not the same as IGS receivers "NISU" and "PTBB."*		

Both satellite- and receiver-clock parameters were estimated in the GPSCPFT analysis; NIST was used as the reference clock relative to which all other clock values were estimated. The data analysis produced one time-transfer value every 300 s. Note that in this paper, we use the term "time-transfer" as shorthand for "time-transfer within a constant," because not all of the GPS links have had their equipment delays measured. Day-boundary discontinuities, i.e., time jumps of 50 ps to 1 ns that occur between the end of one GPSCPFT processing batch and the beginning of the next **[13]**, were not removed or otherwise mitigated. Thus, the GPS time-transfer values can have a discontinuity every 24 h. This will be further discussed later in the paper.

Table 2. GPS Hardware Used in Auxiliary IGS Sites.

Site (IGS code)	Location	GPS receiver	GPS antenna
ALGO	Algonquin Park, Canada	AOA Benchmark ACT	AOAD/M_T
AMC2	Colorado Springs, Colorado, USA	Ashtech Z-XII3T	AOAD/M_T
NLIB	North Liberty, Iowa, USA	AOA SNR-12 ACT	AOAD/M_T + JPLA radome
NRC1	Ottawa, Canada	AOA SNR-12 ACT	AOAD/M_T
OPMT	Paris, France	Ashtech Z-XII3T	3S-02-TSADM
STJO	Saint John's, Newfoundland, Canada	AOA Benchmark ACT	AOAD/M_T
WSRT	Westerbork, Netherlands	AOA SNR-12 ACT	AOAD/M_T + DUTD radome

We examined the agreement of the time-transfer values produced by GPSCPFT and TWSTFT by subtracting the time-transfer values produced by TWSTFT from those produced by GPSCPFT. In performing this subtraction, the GPSCPFT time-transfer value whose time tag most closely matched that of the TWSTFT time-transfer value was used. The GPSCPFT and TWSTFT time tags were within 1 minute of each other. Finally, a constant was subtracted from each of the GPSCPFT-TWSTFT time series.

We examined the combined frequency stability of the GPSCPFT and TWSTFT methods by computing the overlapping Allan deviation $\sigma_y(\tau)$ of the time-difference points [14]. This statistic yielded frequency-stability values out to $\tau = 21$ d 8 h; we applied the statistic *TheoBR* ("bias-removed" *Theo1*) [15] to extend the frequency-stability estimates out to $\tau = 64$ d. The time deviation $\sigma_x(\tau)$ was also computed. All stability statistics were computed using *Stable32 Frequency Stability Analysis Software* [16].

$\sigma_y(\tau)$ is insensitive to a nonzero average value of $y_{GPSCPFT} - y_{TWSTFT}$; in other words, it will not detect a constant difference in the frequency values yielded by the two methods [14]. Therefore, to assess the frequency accuracy of GPSCPFT and TWSTFT, we examined the difference in the frequency values produced by GPSCPFT and TWSTFT for the 10 d, 15 d, and 30 d periods shown in Table 3. Computations were performed using the values shown in Figures 2a-c: for a given period (e.g. MJD 53765-74), the difference between the fractional frequency value obtained from GPSCPFT and that obtained from TWSTFT was computed using endpoints, i.e.,

$$y_{B-A}(t_1,t_2)_{GPSCPFT} - y_{B-A}(t_1,t_2)_{TWSTFT} = \frac{x_{B-A}(t_2)_{GPSCPFT-TWSTFT} - x_{B-A}(t_1)_{GPSCPFT-TWSTFT}}{t_2 - t_1}, \qquad (1)$$

where $x_{B-A}(t)_{GPSCPFT-TWSTFT}$ denotes the difference in the time-transfer estimates obtained from GPSCPFT and TWSTFT for Clock B – Clock A at time t, i.e., the values shown in Figure 2. Each frequency-difference value was assigned a time tag corresponding to the midpoint of the dates over which the frequency difference was computed.

The shortcut of Equation 1 assumes that we would have computed the frequency from GPSCPFT and TWSTFT using the endpoint method ($y[t_1, t_2] = [x(t_2) - x(t_1)]/[t_2 - t_1]$). If we had chosen to use different methods for computing the frequency from TWSTFT and GPSCPFT, then we would have had to compute

$y_{GPSCPFT}$ and y_{TWSTFT} separately before subtracting.

RESULTS

Figures 2a-c show the results of subtracting the GPSCPFT and TWSTFT time-transfer values. No long-term frequency difference between GPSCPFT and TWSTFT is observed.

The day-boundary discontinuities in the METAS-NIST GPSCPFT solutions were typically 100-300 ps in magnitude, which means that every 24 h (or 12 points), there is a jump in the GPSCPFT-TWSTFT values of Figure 2a approximately equal to 10-30 % of a major y-axis division. The day-boundary discontinuities for NPL-NIST (Figure 2b) were similarly sized. The day-boundary discontinuities for PTB-NIST (Figure 2c) were typically 300-600 ps, i.e., 30-60 % of a major y-axis division.

Table 3. Modified Julian Dates Used for 10-Day, 15-Day, and 30-Day Frequency Comparisons.

| 10 days	15 days	30 days
53765-74	53765-79	53765-94
53775-84	53780-94	
53785-94		
53795-804	53795-809	53795-824
53805-14	53810-24	
53815-24		
53825-34	53825-39	53825-54
53835-44	53840-54	
53845-54		
53855-64	53855-69$^{A, C}$	53855-84
53865-74	53860-74^{B}	
53875-84	53870-84$^{A, C}$	
53885-94	53885-99	53885-914
53895-904	53900-14	
53905-14		
53915-24	53915-29	53915-44$^{B, C}$ 53918-47^{A}
53925-34$^{A, B}$ 53927-36^{C}	53930-44$^{B, C}$ 53933-47^{A}	
53935-44^{B} 53937-46^{C} 53938-47^{A}		
^{A}*METAS-NIST* ^{B}*NPL-NIST* ^{C}*PTB-NIST*		
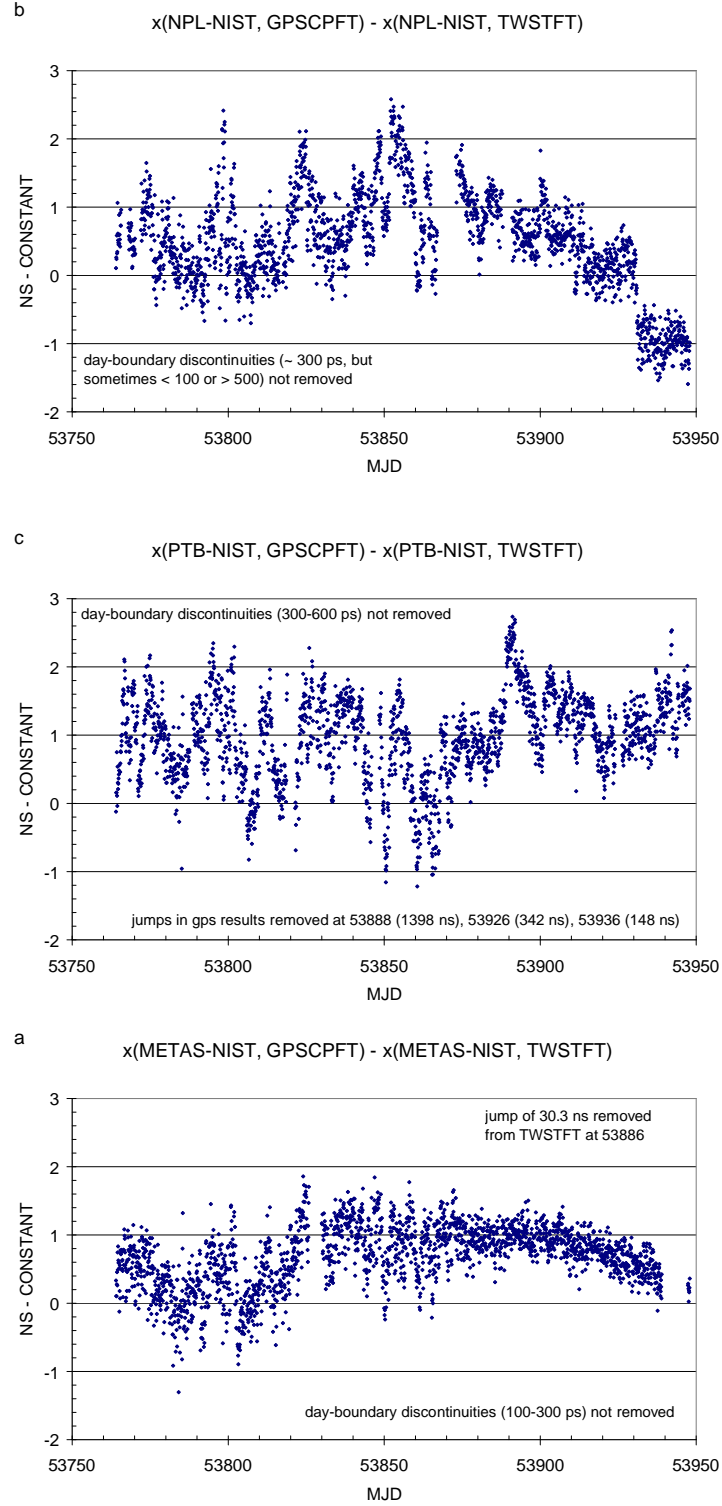
Figure 2. Difference between GPSCPFT and TWSTFT time-transfer values. Aside from data outages, there is one point every 2 hours. An arbitrary constant has been subtracted from each of the plots, i.e., there is no physical significance to the fact that the mean values do not equal zero.

In order to construct Figure 2a (and results derived from it), a discontinuity of 30.3 ns was removed from the METAS-NIST TWSTFT data of MJD 53886 (31 May 2006). This discontinuity was related to problems in the METAS measurement system [17]. The size of the discontinuity was estimated by comparing the GPSCPFT-TWSTFT (time) values before and after the jump. Discontinuities of 1398, 342, and 148 ns were removed from the PTB-NIST GPS time-transfer estimates on MJDs 53888, 53926, and 53936 (2 June, 10 July, and 20 July 2006), respectively (Figure 2c). These jumps were associated with restarts of the PTB GPS receiver [18]. A jump of about 500 ps can be observed in the NPL-NIST differences near MJD 53930 (14 July 2006; Figure 2b). While this jump does occur between the end of one processing batch and the beginning of the next, which would make it consistent with a day-boundary discontinuity, if it were indeed a day-boundary discontinuity, it seems unlikely that the difference values from 53930-47 would remain at this new "lower" value. The origin of this jump is unknown.

The y scales of the Figure 2 plots span 5 ns. This level of noise is comparable to that shown in [3] for the PTB-NIST link. Different receivers were used in [3] than in this experiment. Lahaye *et al.* [4] achieved a y-scale span of only 2 ns for GPSCPFT-TWSTFT along the Paris, France-Colorado USA link OPMT-NISU over a period of 16 d (MJDs 53316-53332; November 2004). We achieve that in the later few months of the METAS-NIST link (Figure 2a).

Figures 3a-b show $\sigma_y(\tau)$, *TheoBR* and $\sigma_x(\tau)$ computed from the time-difference values shown in Figure 2. Due to data outages, stability values were computed using the following subsets of data: METAS-NIST, 53764-938; NPL-NIST, 53772-947; PTB-NIST, 53764-947. Of these subsets, METAS-NIST was missing 75 out of a possible 2100 data points, an outage ratio of 3.6 %. NPL-NIST and PTB-NIST had outage ratios of 151/2112 = 7.1 % and 172/2206 = 7.8 %. Data gaps do not alter *Stable32*'s computation of $\sigma_y(\tau)$, because if one or more of the three phase points needed to compute a frequency difference is missing, *Stable32* ignores that (would-be) contribution to the RMS and moves on to the next frequency-difference point. However, data gaps do alter *Stable32*'s computation of $\sigma_x(\tau)$ in that *Stable32* interpolates the missing phase points prior to computation.

As Figure 3a shows, the combined frequency stability of GPSCPFT and TWSTFT improves with increased averaging time. $\sigma_{y(GPSCPFT) - y(TWSTFT)}$ (τ = 32 h) = 4.8, 5.7, and $6.0 \cdot 10^{-15}$ for METAS-NIST, NPL-NIST, and PTB-NIST, respectively. $\sigma_{y(GPSCPFT) - y(TWSTFT)}$ (τ = 256 h (10 d 16 h)) = 0.7, 1.1, and $1.2 \cdot 10^{-15}$ for METAS-NIST, NPL-NIST, and PTB-NIST. At τ = 512 h (21 d 8 h), these values are 3.5, 4.8, and $6.4 \cdot 10^{-16}$, and at τ = 32 d, *TheoBR* yields 2.6, 4.3, and $4.4 \cdot 10^{-16}$, respectively. The METAS-NIST plot has a slope near -1, which implies combined measurement noise of either white or flicker PM (WHPM; FLPM). NPL-NIST and PTB-NIST have shallower slopes, but are closer to FLPM than random-walk PM/white FM (RWPM; WHFM).

The frequency-stability values shown in Figure 3a are similar to those shown for the PTB-NIST link in [3] and slightly better than those shown for the OPMT-NISU link (2 h ≤ τ ≤ 32 h) in [4]. When we calculate the modified Allan deviation mod $\sigma_y(\tau)$ [14], the stability values we obtain are slightly better than those obtained by [5] along the OPMT-NISU link (MJDs 53304-53329 (October/November 2004)) for τ ≤ 16 h. Our mod $\sigma_y(\tau)$ values are worse than (or sometimes equal to) those obtained by [5] for τ = 32-128 h; this makes sense, because their processing method alleviates day-boundary discontinuities, whereas ours does not.

$\sigma_x(\tau)$ remains below 200 ps for the METAS-NIST link out to 21 d 8 h (Figure 3b). The near-zero slope of the plot implies that the noise type is closer to FLPM than WHPM. The $\sigma_x(\tau)$ values for NPL-NIST and PTB-NIST tend to increase with averaging time, but (again) more slowly than a RWPM/WHFM process would imply. Long-term trends are visible in Figure 2 that would cause $\sigma_x(\tau)$ to increase with time. It is
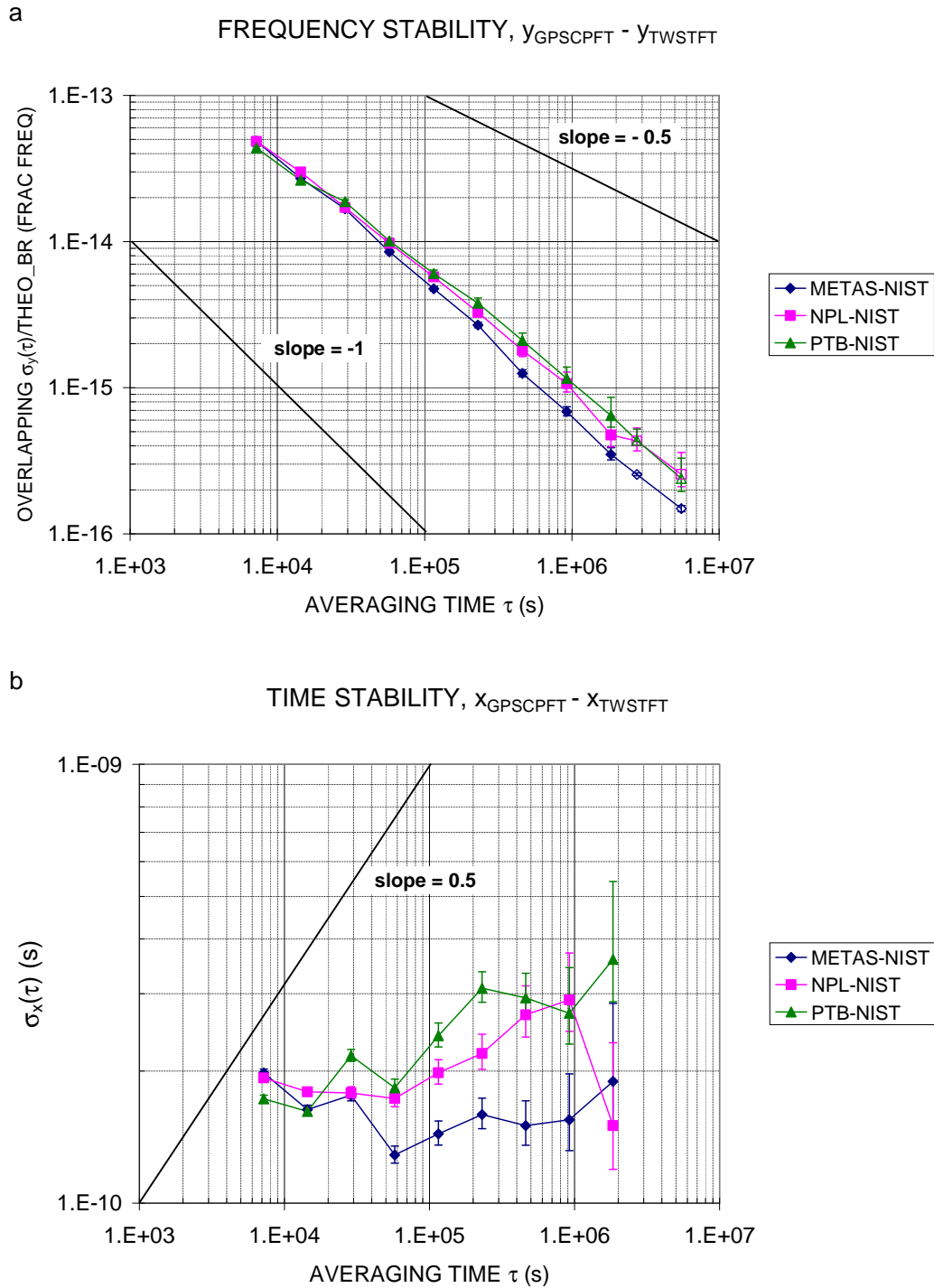
a

FREQUENCY STABILITY, $y_{GPSCPFT}$ - y_{TWSTFT}

b

TIME STABILITY, $x_{GPSCPFT}$ - x_{TWSTFT}

Figure 3. Allan and time deviations of GPSCPFT-TWSTFT values shown in Figure 2. Hollow symbols in (a) indicate values computed using *TheoBR* **[15]** rather than the overlapping Allan deviation **[14]**.

also possible that the upward trend in the PTB-NIST $\sigma_x(\tau)$ reflects imperfect removal of the jumps at MJDs 53888, 53926, and 53936. Regardless, for the most part, the time stability remains less than or equal to 300 ps out to 21 d 8 h. These values of $\sigma_x(\tau)$ are slightly better than those (~ 300-500 ps for $2.3 \leq \tau \leq 74.7$ d) shown in [3]; however, the interpolation used in computing $\sigma_x(\tau)$ may have biased our values low. No time-stability plots were published for the OPMT-NISU link in [4] or [5].

Figures 4a-c show the difference between the frequencies measured using GPSCPFT and those measured using TWSTFT for the epochs shown in Table 3. The agreement of the GPSCPFT- and TWSTFT-derived frequencies obtained for METAS-NIST changes markedly for the better around MJD 53840 (15 April 2006). While $y_{GPSCPFT} - y_{TWSTFT}$ (10 d) was sometimes as large as $1\text{-}2 \cdot 10^{-15}$ before this date, after this it was nearly always less than $5 \cdot 10^{-16}$. The noise level and structure of the subtracted time-transfer values shown in Figure 2a are consistent with this, although in Figure 2a, there appear to be two transitions: one to smaller large-scale structure around MJD 53830, and another to a distinctly lower noise level around MJD 53875 (20 May 2006).

It is not clear what caused these improvements. Neither the GPSCPFT nor the TWSTFT hardware had been changed. However, there are events that correspond to the dates of the structure changes in Figure 3a. On 20 April (MJD 53845), control of the METAS GPS receiver was migrated from a Windows NT to a Windows XP computer. Simultaneously, the software generating the RINEX files was changed from an in-house DOS program to Ashtech's *Geodetic Base Station Software*. It is not known how (or even why) such changes [17] would affect the quality of data. However, the dates of the software change and the transition to better frequency agreement do correspond. It is also possible that the transition to better results was aided by the cessation of a freeze-thaw cycle somewhere in one of the four equipment systems. Figure 5 shows that the diurnals in the METAS-NIST TWSTFT results become smaller as the seasons change from winter to spring, with a visible transition occurring near MJD 53875.

As Figure 4a shows, the value of $y_{GPSCPFT} - y_{TWSTFT}$ of METAS-NIST decreases as the averaging time increases. Therefore, both the frequency stability (Figure 3a) and the frequency accuracy (Figure 4a) improve with increased averaging time. This is true for all three links. The METAS-NIST frequency agreement over periods of 30 d is remarkably good: $1\text{-}3 \cdot 10^{-16}$ in the earlier, noisier part of the experiment, and from $3 \cdot 10^{-17}$ to $2 \cdot 10^{-16}$ in the latter, quieter part of the experiment.

$\sigma_y(\tau)$ is defined as $(1/\sqrt{2})$ times the RMS value of the difference between subsequently measured frequencies. It measures RMS frequency stability. We can compute the RMS of the frequency-accuracy values shown in Figure 4 and then compare accuracy (RMS($y_{GPSCPFT} - y_{TWSTFT}$)) and stability ($\sigma_{y(GPSCPFT) - y(TWSTFT)}(\tau)$). We do not divide RMS($y_{GPSCPFT} - y_{TWSTFT}$) by $\sqrt{2}$ because, for noise processes with correlation times shorter than or equal to that of WHFM, the $1/\sqrt{2}$ in the definition of $\sigma_y(\tau)$ compensates for the fact that the RMS of the <u>subtraction</u> of two (noisy) quantities is computed.

RMS($y_{GPSCPFT} - y_{TWSTFT}$, METAS-NIST, 10 d) $= 7.0 \cdot 10^{-16}$, exactly the same as $\sigma_{y(GPSCPFT) - y(TWSTFT)}$ ($\tau = 10$ d 16 h). RMS($y_{GPSCPFT} - y_{TWSTFT}$, METAS-NIST, 30 d) $= 1.8 \cdot 10^{-16}$, less than both the $\sigma_{y(GPSCPFT) - y(TWSTFT)}$ ($\tau = 21$ d 8 h) and *TheoBR*($\tau = 32$ d) values of 3.5 and $2.6 \cdot 10^{-16}$, respectively. The RMS frequency accuracy appears to be less than or equal to the frequency stability, and hence there appears to be no frequency bias between GPSCPFT and TWSTFT.

The NPL-NIST frequency values produced by GPSCPFT and TWSTFT typically agreed at $0.5\text{-}1.5 \cdot 10^{-15}$ when computed over 10 d intervals (Figure 4b). Again, the agreement is significantly better over 30 d periods, with all $|y_{GPSCPFT} - y_{TWSTFT}|$ values $\leq 5.5 \cdot 10^{-16}$. RMS ($y_{GPSCPFT} - y_{TWSTFT}$, NPL-NIST, 10 d) $= 9.6 \cdot 10^{-16}$, similar to $\sigma_{y(GPSCPFT) - y(TWSTFT)}$ ($\tau = 10$ d 16 h) of $1.1 \cdot 10^{-15}$. RMS ($y_{GPSCPFT} - y_{TWSTFT}$, NPL-NIST, 30

d) = $3.8 \cdot 10^{-16}$, smaller than $\sigma_{y(GPSCPFT)\ -\ y(TWSTFT)}$ (τ = 21 d 8 h) and *TheoBR*(τ = 32 d) of 4.8 and $4.3 \cdot 10^{-16}$, respectively. The curvature of the plot of the 30 d values suggests that a twice per year periodic effect is at work here. A longer data set is needed to observe whether this trend continues.

The quantity $y_{GPSCPFT}$ − y_{TWSTFT}, PTB-NIST, 10 d often reached $1.5\text{-}2 \cdot 10^{-15}$ in the early months of the experiment. However, it became smaller as the experiment progressed, with a resulting RMS value of $1.1 \cdot 10^{-15}$. $\sigma_{y(GPSCPFT)\ -\ y(TWSTFT)}$ (τ = 10 d 16 h) was nearly the same: $1.2 \cdot 10^{-15}$. The agreement between $y_{GPSCPFT}$ and y_{TWSTFT} improves with increased averaging time, and for averaging times of 30 d, except for the first value at MJD 53780, $|y_{GPSCPFT} - y_{TWSTFT}| < 2 \cdot 10^{-16}$. RMS($y_{GPSCPFT}$ − y_{TWSTFT}, PTB-NIST, 30 d) = $2.5 \cdot 10^{-16}$. Although this value is skewed by the point at MJD 53780, it is smaller than the values of $\sigma_{y(GPSCPFT)\ -\ y(TWSTFT)}$ (τ = 21 d 8 h) and *TheoBR*(τ = 32 d), respectively 6.4 and $4.4 \cdot 10^{-16}$, which also would have been biased high by the earlier, noisier values.

As a final test for small frequency biases between GPSCPFT and TWSTFT, we computed the mean, μ, and the standard deviation of the mean, σ_μ, for the nine time series shown in Figures 4a-c. σ_μ was computed by dividing the standard deviation of the time series by $\sqrt{N}$, where N is the number of points in each time series. The results are shown on each plot. The mean values of $y_{GPSCPFT}$ − y_{TWSTFT} range from $1.4 \cdot 10^{-17}$ to $1.9 \cdot 10^{-16}$, with the uncertainties of the means always larger than the means themselves. The largest sum of $\mu + \sigma_\mu$ observed was $(1.9 + 2.7) \cdot 10^{-16} = 4.6 \cdot 10^{-16}$ ($y_{GPSCPFT}$ − y_{TWSTFT}, PTB-NIST, 10 d). Thus, over the 6-month period of this study and within this limit, there appeared to be no long-term frequency bias between GPSCPFT and TWSTFT.

DISCUSSION

It is encouraging that the RMS values of $y_{GPSCPFT}$ − y_{TWSTFT} are small (1.8 to $3.8 \cdot 10^{-16}$) at the 30 d averaging time, and that $y_{GPSCPFT}$ − y_{TWSTFT} (30 d) never exceeds $5.5 \cdot 10^{-16}$. If we assign the noise equally to GPSCPFT and TWSTFT, our worst-case-scenario $5.5 \cdot 10^{-16}$ agreement implies that either technique has a frequency-measurement uncertainty of ∼ $3.9 \cdot 10^{-16}$. This level of uncertainty is useful in comparing many PFSs.

It is also encouraging that we are unable to detect any long-term GPSCPFT-TWSTFT frequency bias over the 6 months of this experiment. It would be nice, however, if the values of $y_{GPSCPFT}$ − y_{TWSTFT} could be made considerably and consistently smaller at the 10 d averaging time.

Hackman *et al.* [2] demonstrated $y_{GPSCPFT}$ − y_{TWSTFT} RMS values of a few to several parts in 10^{16} for 6 to 17 d averaging times for two short-term experiments (13 to 17 d apiece) along the PTB-NIST link. In those experiments, the maximum (worst) value of $y_{GPSCPFT}$ − y_{TWSTFT} never exceeded $1 \cdot 10^{-15}$ for $\tau \geq 9$ d. That is better agreement at short timescales than was achieved in the present experiment for PTB-NIST (or any other link). The same GPS receivers and TWSTFT antennae/modems were used at NIST and PTB in both [2] and the present experiment, although the AOA SNR-8000 receiver at NIST received an ACT upgrade in the interim. We hypothesize that superior results were obtained in [2] because the effects of the day-boundary discontinuities were mitigated more effectively. As mentioned previously, the day-boundary discontinuities for PTB-NIST are particularly large, and we have not yet been able to remove or otherwise circumvent them effectively in this experiment, i.e., in a way that yields better results than those shown in Figure 4. This is true for all three links.
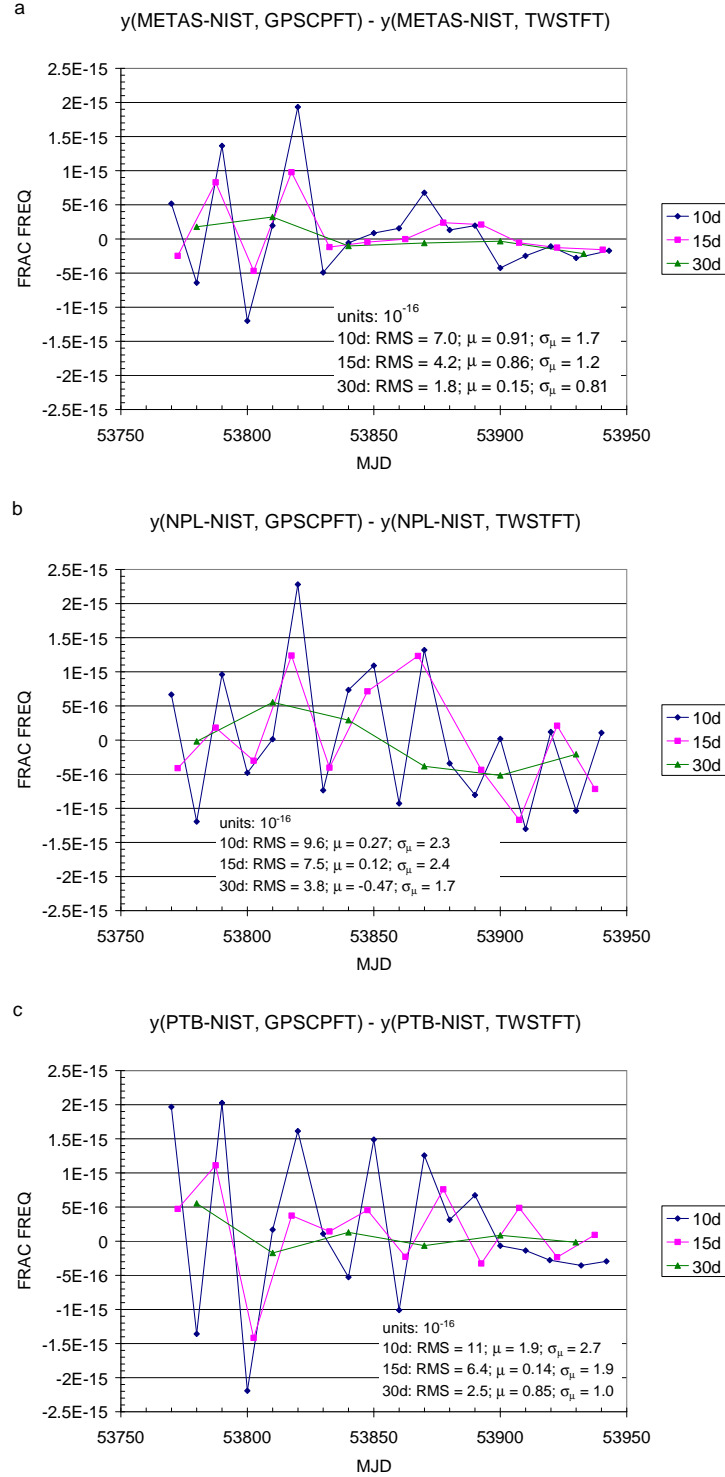
a

y(METAS-NIST, GPSCPFT) - y(METAS-NIST, TWSTFT)

units: 10^{-16}
10d: RMS = 7.0; μ = 0.91; σ_μ = 1.7
15d: RMS = 4.2; μ = 0.86; σ_μ = 1.2
30d: RMS = 1.8; μ = 0.15; σ_μ = 0.81

b

y(NPL-NIST, GPSCPFT) - y(NPL-NIST, TWSTFT)

units: 10^{-16}
10d: RMS = 9.6; μ = 0.27; σ_μ = 2.3
15d: RMS = 7.5; μ = 0.12; σ_μ = 2.4
30d: RMS = 3.8; μ = -0.47; σ_μ = 1.7

c

y(PTB-NIST, GPSCPFT) - y(PTB-NIST, TWSTFT)

units: 10^{-16}
10d: RMS = 11; μ = 1.9; σ_μ = 2.7
15d: RMS = 6.4; μ = 0.14; σ_μ = 1.9
30d: RMS = 2.5; μ = 0.85; σ_μ = 1.0

Figure 4. Difference between frequency values obtained from GPSCPFT and TWSTFT. The RMS, mean (μ) and the uncertainty of the mean (σ_μ) are labeled on each plot for each time series.
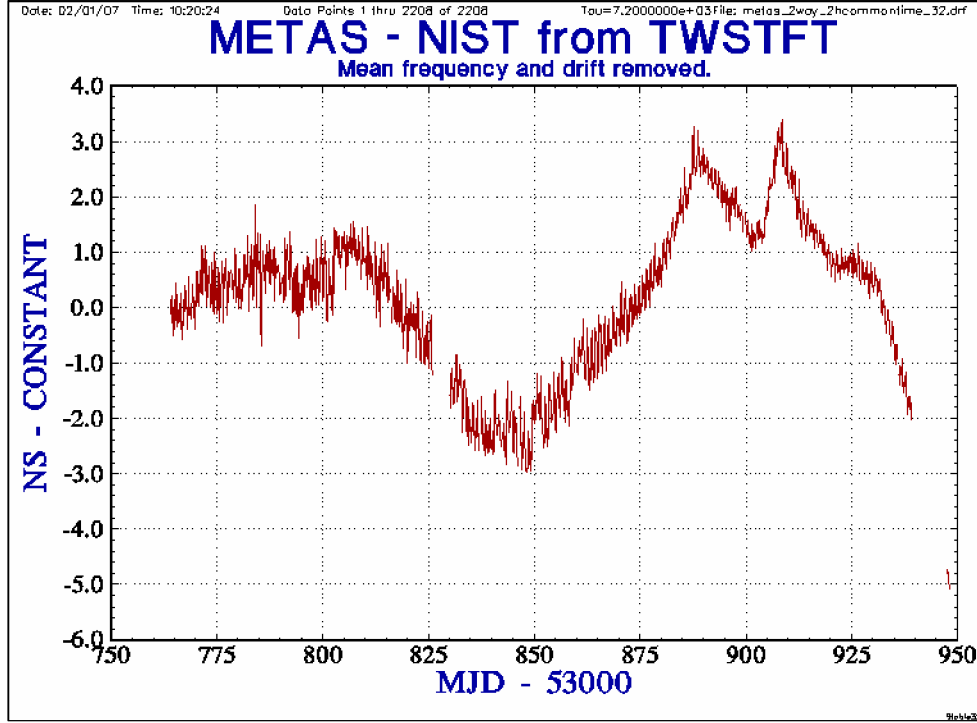
Figure 5. METAS-NIST time-transfer values obtained from TWSTFT 29 Jan – 31 Jul 2006 (drift and frequency offset removed). The diurnals in the TWSTFT values grow smaller as winter becomes spring, with a noticeable transition around MJD 53875.

Work is underway to mitigate the effects of the day-boundary discontinuities in the present experiment. We hope that by doing so, we can reduce the combined uncertainties of GPSCPFT and TWSTFT at shorter (e.g., 10 d) averaging times.

CONCLUSIONS

The frequency values obtained from GPSCPFT and TWSTFT agreed at 1.8 to $3.8 \cdot 10^{-16}$ RMS for 30 d averaging times. No single value of $y_{GPSCPFT} - y_{TWSTFT}$ (30 d) exceeded $5.5 \cdot 10^{-16}$, which would yield $3.9 \cdot 10^{-16}$ frequency accuracy for either GPSCPFT or TWSTFT if the uncertainty were divided equally between the two techniques. RMS frequency-accuracy values were equal to or less than the frequency-stability measure $\sigma_y(\tau)$, and in general, no frequency bias between GPSCPFT and TWSTFT was observed.

The values of $y_{GPSCPFT} - y_{TWSTFT}$ obtained for a given link often varied with time. This was especially noticeable in the $y_{GPSCPFT} - y_{TWSTFT}$ values obtained for averaging times of 10-15 d, with $y_{GPSCPFT} - y_{TWSTFT}$ sometimes becoming as large as $2 \cdot 10^{-15}$. It is not yet clear what caused these variations. The RMS values of $y_{GPSCPFT} - y_{TWSTFT}$ (10 d) ranged from 0.7 to $1.1 \cdot 10^{-15}$, with RMS ($y_{GPSCPFT} - y_{TWSTFT}$ (10 d)) generally equal to $\sigma_{y(GPSCPFT) - y(TWSTFT)}$ (τ = 10 d 8 h).

Some of the noise in y$_{GPSCPFT}$ − y$_{TWSTFT}$ may be due to environmental factors presently beyond our control. Analysis of a longer data set would allow us to investigate how the time-dependent aspects of TWSTFT-GPSCPFT performance evolve. However, we believe that some of the short-term noise is also due to our inability (in the present experiment) to mitigate the effects of day-boundary discontinuities. Better RMS values of y$_{GPSCPFT}$ − y$_{TWSTFT}$ for averaging times of 6 – 17 d were demonstrated in **[2]**, an experiment in which day-boundary discontinuities were effectively managed. We hope to achieve similar (or at least improved) short-term performance once this problem has been resolved.

ACKNOWLEDGMENTS

REFERENCES

[1] T. P. Heavner, S. R. Jefferts, E. A. Donley, J. H. Shirley, and T. E. Parker, 2005, *"NIST-F1: Recent Improvements and Accuracy Evaluations,"* **Metrologia, 42,** 411-422.

[2] C. Hackman, J. Levine, T. E. Parker, D. Piester and J. Becker, 2006, *"A Straightforward Frequency-Estimation Technique for GPS Carrier-Phase Time Transfer,"* **IEEE Transactions on Ultrasonics, Ferromagnetics, and Frequency Control, . UFFC-53,** 1570-1583.

[3] J. F. Plumb and K. M. Larson, 2005, *"Long-Term Comparisons Between Two-Way Satellite and Geodetic Time Transfer Systems,"* **IEEE Transactions on Ultrasonics, Ferromagnetics, and Frequency Control, UFFC-52,** 1912-1918.

[4] F. Lahaye, D. Orgiazzi, P. Tavella, and G. Cerretto, 2006, *"Using Precise Point Positioning for Clock Comparisons,"* **GPS World, 17,** No. 11, pp. 44-49.

[5] A. Bauch, J. Achkar, S. Bize, D. Calonico, R. Dach, R. Hlavac, L. Lorini, T. Parker, G. Petit, D. Piester, K. Szymaniec, and P. Uhrich, 2006, *"Comparison Between Frequency Standards in Europe and the USA at the 10^{-15} Uncertainty Level,"* **Metrologia, 43,** 109-120.

[6] *http://igscb.jpl.nasa.gov*

[7] G. Blewitt, 1989, *"Carrier-Phase Ambiguity Resolution for the Global Positioning System Applied to Geodetic Baselines up to 2000 km,"* **Journal of Geophysical Research, 94,** B8, 10, 187-10, 203.

[8] International Telecommunication Union, 2003, *The Operational Use of Two-Way Satellite Time and Frequency Transfer Employing PN Time Codes*, ITU-R TF.1153-2, Geneva, Switzerland.

[9] F. H. Webb and J. F. Zumberge, eds., 1997, *An Introduction to GIPSY/OASIS-II: Precision Software for the Analysis of Data from the Global Positioning System*, JPL D-11088 (Jet Propulsion Laboratory, Pasadena, California).

[10] IGS precise ephemerides: *http://igscb.jpl.nasa.gov/igscb/product*; igs*.sp3 files from weeks 1360-86 were used. IGS "sinex" coordinates: *http://garner.ucsd.edu/pub/products*; igs06p*.snx files from weeks 1360-86 were used.

[11] *ftp://hpiers.obspm.fr/iers/bul/bulb*; bulletinb.217 through .223 were used.

[12] *http://www.oso.chalmers.se/~loading*.

[13] J. Ray and K. Senior, 2003, *"IGS/BIPM Pilot Project: GPS Carrier Phase for Time/Frequency Transfer and Timescale Formation,"* **Metrologia, 40,** S270-S288.

[14] The Institute of Electrical and Electronics Engineers, 1999, *IEEE Standard Definitions of Physical Quantities for Fundamental Frequency and Time Metrology – Random Instabilities*, IEEE Standard 1139-1999, ISBNs 0-7381-1753-6 (print), 0-7381-1754-4 (pdf), 31 pp. (IEEE, New York).

[15] D. A. Howe, 2006, *"TheoH: a Hybrid, High-Confidence Statistic That Improves on the Allan Deviation,"* **Metrologia, 43,** S322-S331.

[16] *http://www.stable32.com*

[17] L-G. Bernier, 2006, personal communication.

[18] J. Becker, 2006, personal communication.